

Regular Article

Tunable elastic heterogeneity caused by deformation-induced magnetization in flexible metallic glass



B. Huang^a, Q.F. He^a, A.D. Wang^b, C.L. Zhao^b, Q. Wang^c, Y. Yang^{a,*}, C.T. Liu^{a,*}

^a Centre for Advanced Structural Materials, Department of Mechanical and Biomedical Engineering, City University of Hong Kong, Tat Chee Avenue, Kowloon Tong, Kowloon, Hong Kong, China

^b Key Laboratory of Magnetic Materials and Devices, Ningbo Institute of Materials Technology and Engineering, Chinese Academy of Sciences, Ningbo, Zhejiang 315201, China

^c Laboratory for Microstructures, Institute of Materials Science, Shanghai University, Shanghai 200072, China

ARTICLE INFO

Article history:

Received 6 October 2016

Received in revised form 1 November 2016

Accepted 1 November 2016

Available online 8 November 2016

Keywords:

Metallic glass

Magnetic force microscopy

Nanoindentation

Magnetomechanical interaction

ABSTRACT

In this letter we explore the magnetization effect on mechanical properties of a ductile $\text{Fe}_{83}\text{C}_1\text{B}_{11}\text{Si}_2\text{P}_3$ metallic glass (MG). We firstly demonstrate that magnetic anisotropy can be systematically created by plastic deformation using high-load Berkovich indentation, and then provide compelling evidence by subsequent spherical nanoindentation which reveals tunable magnetization-induced submicron elastic heterogeneity. A new mechanism of magnetomechanical interaction, different from the alteration of “flow defect”, is proposed for explaining the apparent softening in the region without plastic deformation. Our studies have significance for modification and controlling of the microstructure and mechanical properties of MGs with respect to magnetic effect.

© 2016 Acta Materialia Inc. Published by Elsevier Ltd. All rights reserved.

The nanoscale structural and mechanical heterogeneity of metallic glasses (MGs) has been revealed and intensively studied by atomic force microscopy [1,2], nanoindentation [3] and other techniques [4,5]. Due to their metastable nature, the local structure and mechanical properties of MGs can be tuned by adjusting their thermal/mechanical histories through methods with a few thermo-mechanical variables, such as plastic deformation [6,7], changing cooling rate [8] and heat treatment [8,9]. For example, it was reported that severe plastic deformation caused by cold rolling [10,11], indentation [12] and high pressure torsion [13] can significantly soften MGs. Usually, such a property change was attributed to the introduction or annihilation of “flow defect” in the amorphous structure, such as free volume [14], shear transformation zone (STZ) [15], liquid-like region [4], flow unit [16] and so on [5]. However, it is noteworthy that the variation of “flow defect” is not the only mechanism that causes softening in MGs. For those with a non-zero magnetostriction coefficient (λ), magnetization can also change the microstructure and thus the mechanical properties [17–19]. In general, the magnetization can be induced by applied stress and/or magnetic field [17–19]. However, the magnetization effect on the microstructure and mechanical properties of macroscopically homogeneous MGs has been scarcely studied. In this letter, we use nanoindentation to study the magnetization effect on the mechanical properties of a model ductile $\text{Fe}_{83}\text{C}_1\text{B}_{11}\text{Si}_2\text{P}_3$ MG ribbon [20]. Submicron elastic

heterogeneity is revealed in the stress-concentrated region without plastic deformation, and a mechanism of magnetomechanical interaction is proposed for explaining the obvious softening phenomenon.

$\text{Fe}_{83}\text{C}_1\text{B}_{11}\text{Si}_2\text{P}_3$ MG ribbon with good ductility with a thickness of 40 μm was fabricated in argon atmosphere with the single copper roller melt-spinning method at the wheel speed of 20 m/s. The fully amorphous structure of the ribbon was confirmed through X-ray diffraction (see Fig. S1 in the supplementary material). Different from the free surface, the side of the ribbon contacting with the roller during the preparation is full of surface irregularities and contains uncertain internal stress inhomogeneity. To create magnetic domain patterns in a controlled manner, a pattern of micro-indentations was made on the flat and clean untreated free surface of the as spun ribbon through Berkovich indentation on the TI 950 TriboIndenter system (Hysitron Inc., Minneapolis, MN). The surface morphology and magnetic domain structure within the indentation pattern were then examined by the Dimension Icon® Magnetic Force Microscopy (MFM) under the LiftMode with a constant lift height of 150 nm. The mechanical properties inside the high-load indentation pattern were then measured with the low-load spherical indentation with a tip radius R of 184 nm at room temperature.

Fig. 1(a) shows the load-displacement (P - h) curves stemming from the programmed loading-holding-loading profile [the inset of Fig. 1(a)] with the Berkovich sharp indenter at the maximum load of 1 N. Consequently, significant shear bands (SBs) can be observed near the side of the triangle residual indentation at the surface of $\text{Fe}_{83}\text{C}_1\text{B}_{11}\text{Si}_2\text{P}_3$ ribbon suggesting plastic deformation [Fig. 1(b)]. A square pattern with four residual indentations labeled as 1, 2, 3 and 4 was created by

* Corresponding authors.

E-mail addresses: yonyang@cityu.edu.hk (Y. Yang), chainliu@cityu.edu.hk (C.T. Liu).

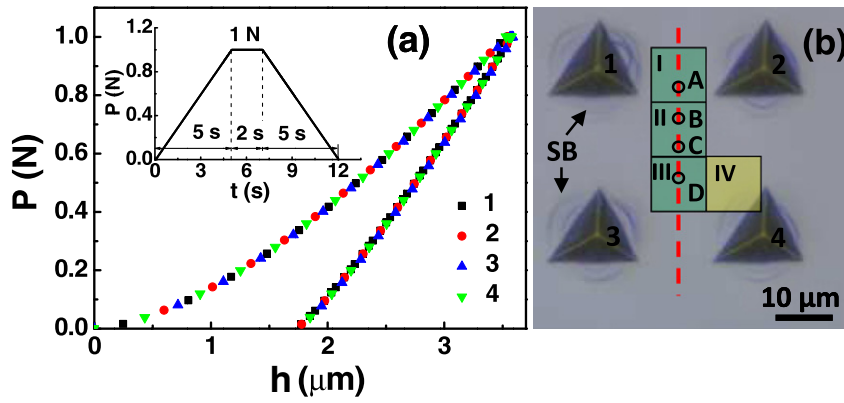


Fig. 1. (a) The P - h curves for four indentations of the square pattern with the inset showing the load-time (P - t) procedure for each indentation. (b) The optical microscopic image of the pattern with the indentations spaced as $30\ \mu\text{m}$. The indentations are labeled as 1, 2, 3 and 4. The squares I, II, III and IV mark the regions detected with MFM. The circles A, B, C and D mark the nanoindentation positions, and the dashed line is the guide line.

positioning the indentations $30\ \mu\text{m}$ apart [Fig. 1(b)]. It is worth noting that the P - h curves for all the indentations override each other implying the uniformity of the MG ribbon at the micrometer scale.

The magnetic properties of the pristine and indented surface of the MG ribbon were examined with MFM. The phase image of the as spun

ribbon is shown in Fig. 2(a). The phase degree varies between -0.18° and 0.18° , and no magnetic domain pattern is found within the resolution of MFM. The phase images of regions I, II and III marked by the green squares in Fig. 1(b) are shown in Fig. 2(b), (c) and (d), respectively. A strip-like magnetic domain pattern with a width less than $200\ \text{nm}$

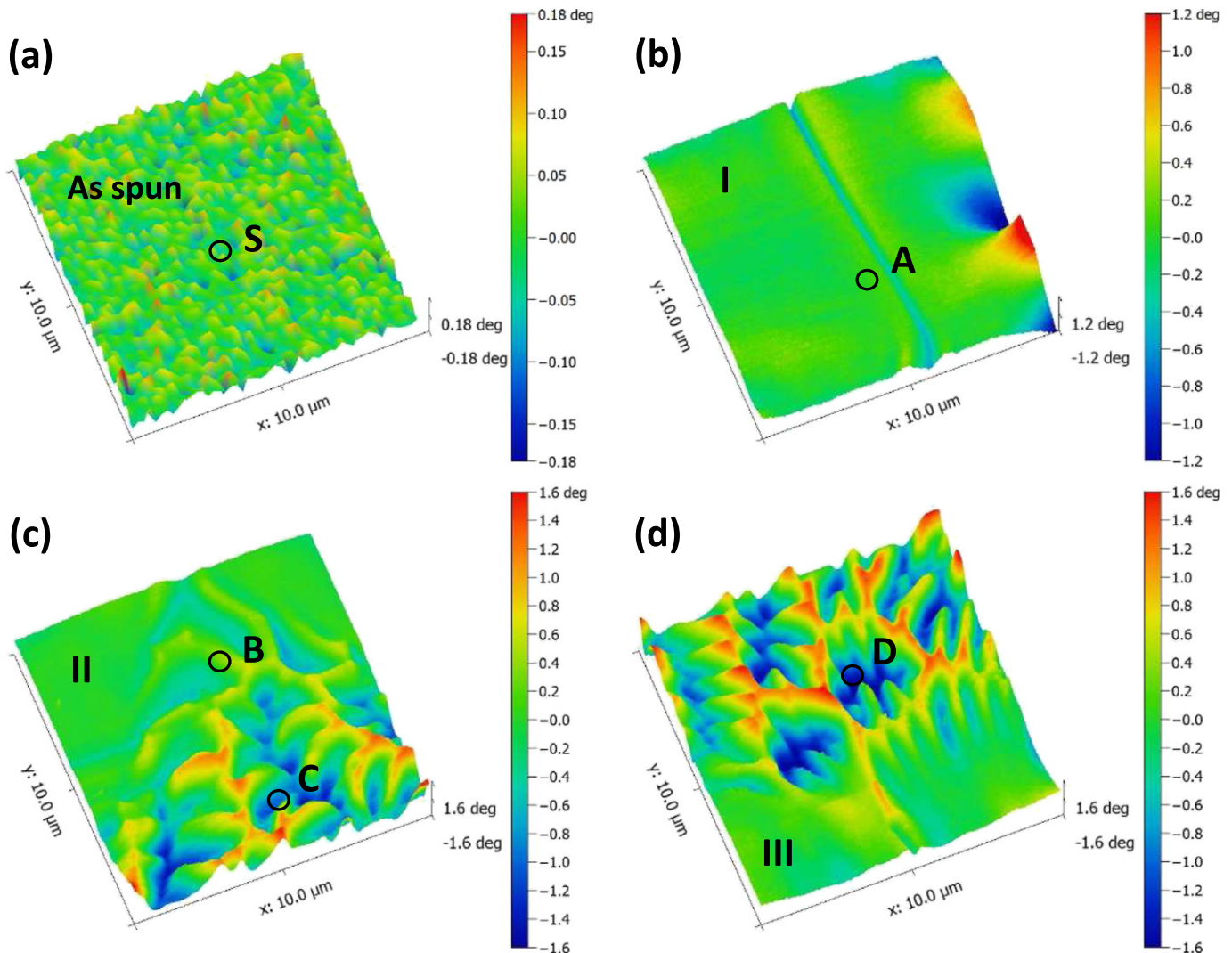


Fig. 2. The phase images of (a) as spun $\text{Fe}_{83}\text{C}_1\text{B}_{11}\text{Si}_2\text{P}_3$ ribbon, (b) region I, (c) region II and (d) region III of deformed $\text{Fe}_{83}\text{C}_1\text{B}_{11}\text{Si}_2\text{P}_3$ ribbon detected with MFM. The circles S, A, B, C and D mark the nanoindentation positions.

runs through region I and connects the dendritic pattern of region II. The dendritic pattern becomes more apparent with the phase degree difference over 3° in region III. The branch width of the dendritic patterns ranges from several hundred nanometers to several microns. Note that the blue color herein indicates the magnetization direction in the area is nearly parallel to the upward tip magnetization while the red color means the opposite [21]. Thus, regular magnetic anisotropy perpendicular to the sample surface was induced by plastic deformation through high-load indentation patterning.

To clarify the formation of the domain patterns the height and phase images of region IV marked by the yellow square in Fig. 1(b) are shown in Fig. 3(a) and (b). A deformation-induced hump with a height of over 200 nm containing SBs appears near the side of the triangle indentation indicating the existence of compressive stress parallel to the surface. Meanwhile, the top-left area of region IV bearing the compressive stress seems higher than the top-right and down-left areas. Corresponding to the surface topography, a spot-like magnetic domain pattern appears in the plastically deformed region, and a wave-like pattern emerges in the spreading direction of the compressive stress pointing to region II and III (marked by the red arrow). The magnetoelastic energy (E_{ME}) can be expressed as $E_{ME} = -3\lambda\sigma\cos^2\theta/2$, where σ is the magnitude of the applied stress and θ is the angle between the directions of the applied stress and the magnetic domain vector [22]. To reduce E_{ME} , the magnetic domain vector is prone to align parallel or antiparallel to the tensile stress and perpendicularly to the compressive stress. Therefore, the

formation of the regular submicron local magnetic anisotropy in the normal direction [as shown in Fig. 2(b), (c) and (d)] is to minimize E_{ME} to adapt to the concentrated compressive stresses emitted from the plastically deformed region of the high-load indentations [23].

We further performed nanoindentation on the as spun and deformed ribbons to study the deformation effect on the elastic properties of the MG. Fig. 4(a) shows the nanoindentation unloading curves with the peak load of 80 μN on the as spun and deformed ribbons [The nanoindentation positions S, A, B, C, and D far from plastically deformed regions are marked by the black circles in Fig. 1(b), Fig. 2(a)–(d)]. With complete unloading, the displacement h returns to zero conforming to elastic deformation. The maximum displacement h_{max} at the same peak load of 80 μN becomes larger and larger when the position moves from S to A, B, C and D. The hardness H of the as spun ribbon was detected as 11.1 ± 0.2 GPa with the nanoindentation method. Fig. 4(b) shows the H at different positions of the deformed ribbon. With the position moving from A to D, H decreases from 10.7 ± 0.2 GPa to 8.5 ± 0.7 GPa. The phenomenon implies the elastic heterogeneity with apparent softening inside the indentation pattern of the deformed Fe-based MG.

We plot the h versus $P^{2/3}$ curve for the unloading nanoindentation data at different positions to further analyze the softening effect [as shown in Fig. 4(c)]. Applying “the rule of mixture”, the E of $\text{Fe}_{83}\text{C}_1\text{B}_{11}\text{Si}_2\text{P}_3$ MG can be estimated as 234 GPa [8]. The unloading curve (the solid olive line) at position S of the as spun ribbon can be well fitted with the Hertzian theory (h equals to h_{ela} , i.e., the displacement caused by elastic effect) [24], i.e.,

$$h_{\text{ela}} = \left[3P(1-\nu^2)/4R^{1/2}E \right]^{2/3}. \quad (1)$$

Through the fitting of the unloading curve with Eq. (1) (the dashed olive line), the ν of $\text{Fe}_{83}\text{C}_1\text{B}_{11}\text{Si}_2\text{P}_3$ MG is obtained as 0.400 close to that of $\text{Fe}_{80}\text{P}_{13}\text{C}_7$ MG [8]. However, the unloading curves at the positions A, B, C and D of the deformed ribbon (the solid red, blue, green and magenta lines) deviate from the Hertzian theory and cannot be fitted with Eq. (1). From the position S to A, B, C and D, the slope at the low P region becomes larger and larger, which implies the decrease of E and the increase of softening effect. With the increasing applied load P , the curve gradually becomes parallel to the dashed olive line, and the E approaches 234 GPa.

We made the same pattern with indentations equally spaced 30 μm apart on the as spun Vit105 ($\text{Zr}_{52.5}\text{Cu}_{17.9}\text{Ni}_{14.6}\text{Al}_{10}\text{Ti}_5$ MG) ribbon and obtained the unloading curve from the sphere indentation at the same position as D in Fig. 1(b) [the black line in Fig. 4(c)]. With the reported Young's modulus $E = 85$ GPa and Poisson's ratio $\nu = 0.372$ [8], the h versus $P^{2/3}$ curve can be well fitted with the Hertzian theory, i.e., Eq. (1). This behavior indicates that the abnormal softening and deviation from the Hertzian theory observed for the deformed Fe-based MG cannot be found in nonmagnetic MG and are not caused by the deformation-induced “flow defect”. Furthermore, as the absolute value of phase degree increases systematically with the elastic softening across the positions from S to A, B, C and D [Fig. 2(a)–(d)], we conclude that the abnormal elastic heterogeneity of the deformed Fe-based MG could relate to the stress-induced magnetic anisotropy.

We can simply take the Fe-based soft magnetic MG as a “composite” consisting of an ideal elastic “matrix” and dispersed unsymmetrical magnetic moments. By taking into account the magnetoelastic and elastic effects, the total elastic displacement at the load P can be derived as

$$h(P) = h_{\text{mag}} + h_{\text{ela}}, \quad (2)$$

where h_{mag} represents the displacement caused by magnetostriction. To simplify our further analysis, we use $\bar{\sigma}_0$ and $\bar{\sigma}_1$ to represent the averaged local residual stress and applied stress under the contact area of the sphere indenter, which have the same average mechanical effect

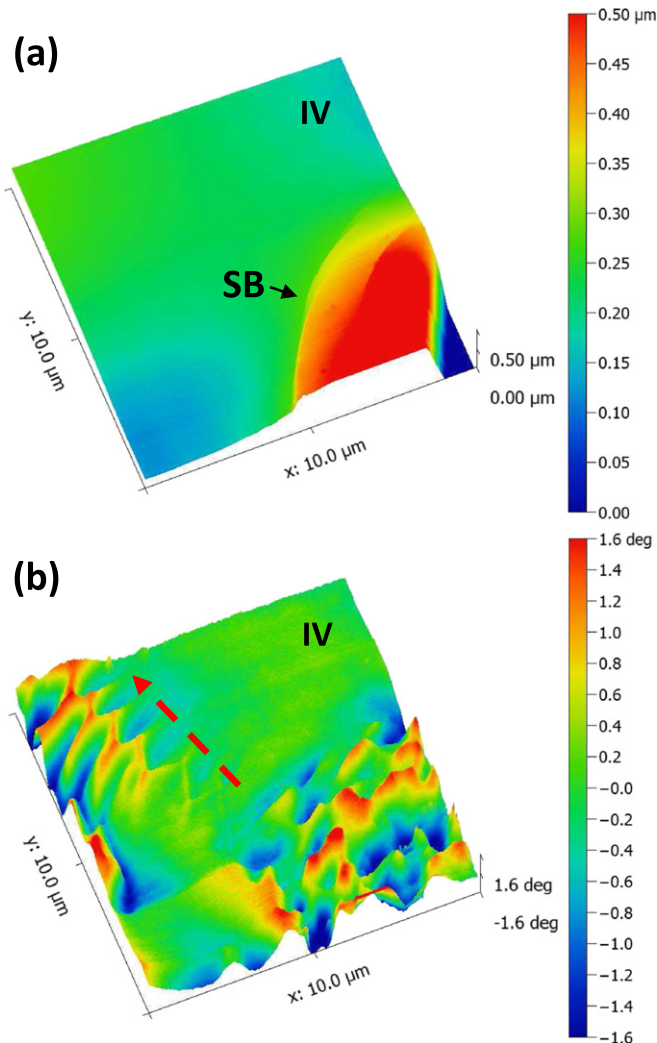


Fig. 3. (a) The height and (b) phase images of region IV of deformed $\text{Fe}_{83}\text{C}_1\text{B}_{11}\text{Si}_2\text{P}_3$ ribbon detected with MFM. The arrow marks the direction of the stress.

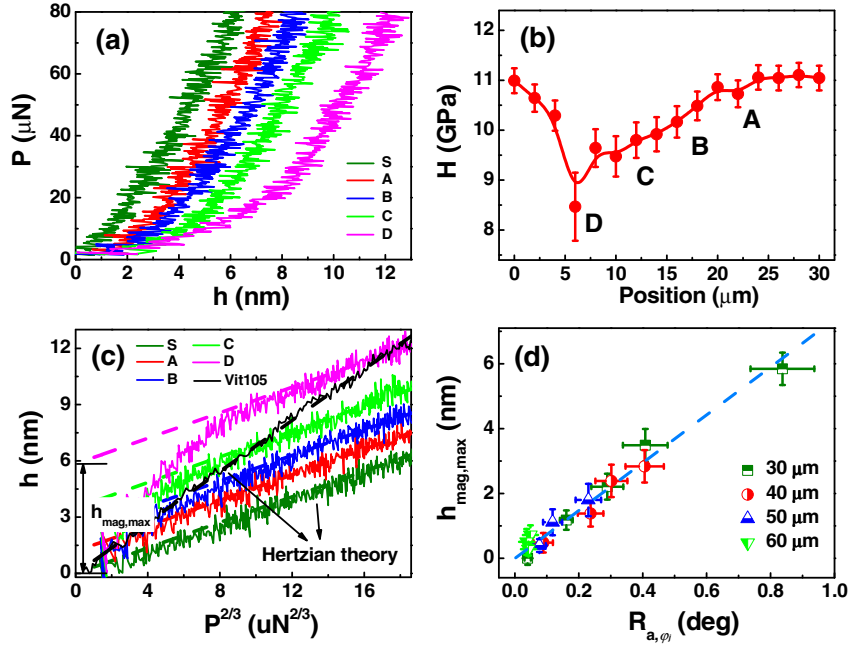


Fig. 4. (a) The nanoindentation unloading curve at the positions S, A, B, C and D. (b) The hardness H at different positions along the dashed line in Fig. 1(b). (c) The $P^{2/3}$ dependent h unloading curve at the positions S, A, B, C and D of $\text{Fe}_{83}\text{C}_1\text{B}_{11}\text{Si}_2\text{P}_3$ ribbon and on deformed Vit105. The dashed line is the fitting line with its intercept as $h_{\text{mag,max}}$. (d) The $R_{a,\varphi}$ dependent $h_{\text{mag,max}}$ at different positions for deformed $\text{Fe}_{83}\text{C}_1\text{B}_{11}\text{Si}_2\text{P}_3$ ribbon with the indentations spaced as $30\ \mu\text{m}$, $40\ \mu\text{m}$, $50\ \mu\text{m}$ and $60\ \mu\text{m}$. The dashed line is the guide line.

as the real complex distributed stresses. Thus, $h_{\text{mag}} = l[\varepsilon_{\text{m}}(\bar{\sigma}_0 + \bar{\sigma}_1) - \varepsilon_{\text{m}}(\bar{\sigma}_0)]$, where l denotes the largest depth of the region affected by magnetoelastic effect at the peak load of $80\ \mu\text{N}$. The magnetic strain ε_{m} under the stress σ can be expressed as

$$\varepsilon_{\text{m}}(\sigma) = \frac{\int_0^\pi \frac{3}{2} \lambda \left(\cos^2 \theta - \frac{1}{3} \right) \exp \left[\left(-\frac{3}{2} \lambda \sigma \cos^2 \theta \right) / \Omega \right] \sin \theta d\theta}{\int_0^\pi \exp \left[\left(-\frac{3}{2} \lambda \sigma \cos^2 \theta \right) / \Omega \right] \sin \theta d\theta} \quad (3)$$

where Ω is an empirical factor that accounts for local fluctuations [25]. From Eq. (3), we can find that when $\sigma \rightarrow -\infty$, $\varepsilon(\sigma) \rightarrow -\lambda/2$, and when $\sigma \rightarrow +\infty$, $\varepsilon(\sigma) \rightarrow \lambda$. In the nanoindentation process, when $\bar{\sigma}_1$ is sufficiently large, h_{mag} approaches a saturated value. Therefore, h shows a linear relation with $P^{2/3}$ when P is large, as shown in Fig. 4(c) (the solid lines). With the fitting of the line at large P (the dashed line) with Eq. (2), we get the maximum displacement $h_{\text{mag,max}}$ induced by magnetostriction under $80\ \mu\text{N}$ from S to A, B, C and D [the intercept value on the h axis when $P^{2/3}$ equals to zero in Fig. 4(c)]. The increasing softening and deviation from the Hertzian theory are caused by the increasing $h_{\text{mag,max}}$.

We use the average roughness R_{a,φ_j} of the magnetic phase image to gauge the local strength of magnetization in the normal direction of the ribbon, which is defined as $R_{a,\varphi_j} = (1/N) \sum_{j=1}^N |\phi_j|$ with φ_j the phase degree at the point of j and N the number of data [21]. For the ribbon with $30\ \mu\text{m}$ -spaced indentations, the fitted $h_{\text{mag,max}}$ increases with R_{a,φ_j} at the nanoindentation region as shown in Fig. 4(d). From S to D, $h_{\text{mag,max}}$ increases from $0.0 \pm 0.2\ \text{nm}$ to $5.8 \pm 0.5\ \text{nm}$ as R_{a,φ_j} increases from $0.04 \pm 0.01^\circ$ to $0.84 \pm 0.10^\circ$. We also made patterns with four indentations equally spaced at a distance of $40\ \mu\text{m}$, $50\ \mu\text{m}$ and $60\ \mu\text{m}$ on the as spun ribbon, and measured the magnetic and local mechanical properties at the surface with the same method described above. The height and phase images in the middle of different patterns are shown in Fig.

S2 in the supplementary material. With the fitting of the nanoindentation curve (as shown in Fig. S3 in the supplementary material) at large P we obtain $h_{\text{mag,max}}$ at different positions. At all the nanoindentation positions $h_{\text{mag,max}}$ increases almost linearly with R_{a,φ_j} as indicated by the dashed line in Fig. 4(d). The small R_{a,φ_j} on the ribbon with indentations of a larger spacing indicates less magnetic moments lying perpendicular to the surface at the local regions, which is consistent with the small compressive residual stress in this case. This behavior further supports that the elastic heterogeneity with softening inside the indentation pattern of Fe-based MG is caused by the deformation-induced magnetization. The induced elastic heterogeneity is at the submicron scale corresponding to the magnetic domain sizes in Fig. 2(b)–(d).

As the largest $h_{\text{mag,max}}$ in our experiments reaches $5.8 \pm 0.5\ \text{nm}$, we can estimate that the local λ in the thickness direction should exceed $80\ \text{ppm}$ based on Eqs. (2) and (3), much larger than the macroscopic λ ($\sim 20\ \text{ppm}$) reported for other Fe-based MGs or pure Fe [26]. Aside from the chemical effect, another mechanism of magnetostriction enhancement is associated with the heterogeneous structure as discovered in FeGa and CoFe alloys [27–29]. Structural transformation of D03 nanoprecipitates embedded in the A2 matrix results in a large λ over $200\ \text{ppm}$ in the [100] crystallographic direction in the FeGa crystal [27,28]. The upper limit of magnetostriction λ_{100} of CoFe alloy can even reach above $1000\ \text{ppm}$ due to the precipitation of an equilibrium Co-rich face-centered cubic phase embedded in a Fe-rich body-centered cubic matrix [29]. The local λ above $80\ \text{ppm}$ of $\text{Fe}_{83}\text{C}_1\text{B}_{11}\text{Si}_2\text{P}_3$ MG underlying the obvious magnetization-induced softening might manifest a possible transformation or precipitation of some type of nanoclusters with orientation anisotropy caused by the ribbon fabrication process [30], the details of which however warrant further investigation.

In summary, we create regular magnetic anisotropy through plastic deformation of ductile $\text{Fe}_{83}\text{C}_1\text{B}_{11}\text{Si}_2\text{P}_3$ MG. Submicron elastic heterogeneity is discovered in the region without plastic deformation. We demonstrate that the elastic softening is caused by the deformation-induced magnetization rather than the alteration of “flow defect”. The studies provide new insights into the modification and controlling of the

microstructure and mechanical properties of MGs with respect to magnetic effect.

Acknowledgements

The research of Y. Y. and C. T. L. is supported by the Hong Kong Government through the General Research Fund (GRF) with the grant number CityU11214914 and CityU11207215, respectively. Useful discussions with B. A. Sun and Y. M. Lyv are appreciated.

Appendix A. Supplementary data

See supplementary material for the XRD pattern of as spun $\text{Fe}_{83}\text{C}_1\text{B}_{11}\text{Si}_2\text{P}_3$ ribbon, the height and phase images, and nanoindentation curves of $\text{Fe}_{83}\text{C}_1\text{B}_{11}\text{Si}_2\text{P}_3$ ribbons with indentations spaced at a distance of 40 μm , 50 μm and 60 μm . Supplementary data associated with this article can be found in the online version, at <http://dx.doi.org/10.1016/j.scriptamat.2016.11.001>.

References

- [1] H. Wagner, D. Bedorf, S. Kuchemann, M. Schwabe, B. Zhang, W. Arnold, K. Samwer, *Nat. Mater.* 10 (2011) 439–442.
- [2] Y.H. Liu, D. Wang, K. Nakajima, W. Zhang, A. Hirata, T. Nishi, A. Inoue, M.W. Chen, *Phys. Rev. Lett.* 106 (2011) 125504.
- [3] D. Pan, A. Inoue, T. Sakurai, M.W. Chen, *Proc. Natl. Acad. Sci. U. S. A.* 105 (2008) 14769–14772.
- [4] J.C. Ye, J. Lu, C.T. Liu, Q. Wang, Y. Yang, *Nat. Mater.* 9 (2010) 619–623.
- [5] T. Ichitsubo, E. Matsubara, T. Yamamoto, H.S. Chen, N. Nishiyama, J. Saida, K. Anazawa, *Phys. Rev. Lett.* 95 (2005) 245501.
- [6] S. Xie, E.P. George, *Acta Mater.* 56 (2008) 5202–5213.
- [7] A.L. Greer, Y.Q. Cheng, E. Ma, *Mater. Sci. Eng. R* 74 (2013) 71–132.
- [8] W.H. Wang, *Prog. Mater. Sci.* 57 (2012) 487–656.
- [9] S.V. Ketov, Y.H. Sun, S. Nachum, Z. Lu, A. Checchi, A.R. Beraldin, H.Y. Bai, W.H. Wang, D.V. Louzguine-Luzgin, M.A. Carpenter, A.L. Greer, *Nature* 524 (2015) 200–203.
- [10] H. Bei, S. Xie, E.P. George, *Phys. Rev. Lett.* 96 (2006) 105503.
- [11] M. Stolpe, J.J. Kruzic, R. Busch, *Acta Mater.* 64 (2014) 231–240.
- [12] R. Bhowmick, R. Raghavan, K. Chattopadhyay, U. Ramamurty, *Acta Mater.* 54 (2006) 4221–4228.
- [13] F. Meng, K. Tsuchiya, I. Seichiro, Y. Yokoyama, *Appl. Phys. Lett.* 101 (2012) 121914.
- [14] F. Spaepen, *Acta Metall.* 25 (1977) 407–415.
- [15] M.L. Falk, J.S. Langer, *Phys. Rev. E* 57 (1998) 7192.
- [16] Z. Wang, P. Wen, L.S. Huo, H.Y. Bai, W.H. Wang, *Appl. Phys. Lett.* 101 (2012) 121906.
- [17] E.W. Lee, *Rep. Prog. Phys.* 18 (1955) 184.
- [18] R.C. O'Handley, C.P. Chou, *J. Appl. Phys.* 49 (1978) 1659.
- [19] Z. Kaczowski, *Mater. Sci. Eng. A* 226 (1997) 614–625.
- [20] A. Wang, C. Zhao, H. Men, A. He, C. Chang, X. Wang, R.-W. Li, *J. Alloys Compd.* 630 (2015) 209–213.
- [21] U. Hartmann, *Annu. Rev. Mater. Sci.* 29 (1999) 53–87.
- [22] E.D.T. De Lacheisserie, *Magnetostriction: theory and applications of magnetoelasticity*, CRC, New York, 1993.
- [23] J. Stöhr, H.C. Siegmann, *Magnetism. From fundamentals to nanoscale dynamics*, Springer, Berlin, 2006.
- [24] A.C. Fischer-Cripps, *Introduction to contact mechanics*, Springer, New York, 2000.
- [25] S. Datta, J. Atulasimha, C. Mudivarthi, A.B. Flatau, *J. Magn. Magn. Mater.* 322 (2010) 2135–2144.
- [26] B. Shen, M. Akiba, A. Inoue, *Appl. Phys. Lett.* 88 (2006) 131907.
- [27] A.G. Khachaturyan, D. Viehland, *Metall. Mater. Trans. A* 38 (2007) 2308–2316.
- [28] A.G. Khachaturyan, D. Viehland, *Metall. Mater. Trans. A* 38 (2007) 2317–2328.
- [29] D. Hunter, W. Osborn, K. Wang, N. Kazantseva, J. Hatrick-Simpers, R. Suchoski, R. Takahashi, M.L. Young, A. Mehta, L.A. Bendersky, *Nat. Commun.* 2 (2011) 518.
- [30] T. Nakamura, H. Koshiba, M. Imafuku, A. Inoue, E. Matsubara, *Mater. Trans.* 43 (2002) 1918–1920.